CHAPTER III

OMES-WSPHS INTEGRATION CONSIDERING PRICING MECHANISM UNDER TOC MINIMIZATION

3.1 General Introduction

This chapter focuses on the integration of OMES-WSPHS under a pricing mechanism to minimize the TOC. The study aims to enhance the efficiency of energy dispatch by coordinating multiple energy sources, including the electricity grid, NG, WTs, PVPs, and HS. The proposed system integrates hydrogen storage as a key element to optimize energy utilization by converting excess RE into hydrogen, which can later be used for electricity generation. To achieve the optimal scheduling of the system, the PSO-LP method is employed. This optimization technique enables effective coordination between multiple energy sources while considering the TOU tariff and real-time pricing (RTP). The study explores various case studies to evaluate the impact of different operational scenarios, including the presence or absence of HS, coordinated and uncoordinated operations between electricity and NG, as well as cases with and without solar power integration. The results provide insights into how integrating HS and optimizing energy dispatch strategies can contribute to cost reduction and improved energy management.

3.2 Problem Formulation

3.2.1 System Modeling

For system modeling, the components of MES-WSPHS are shown in Fig. 3.1. The input part consists of an electricity grid and NG to dispatch energy to the output which is electricity and heat demands. Conversion technology, which is the center of EH includes a transformer (TR), gas boiler (GB), micro-turbine (MT), WTs, and

PVPs. With HS, the excessive RE can be converted to hydrogen and stored for utilization at the proper period. As a result, the resources can be coordinately utilized, leading to higher overall efficiency. Electricity (P_E) and NG (P_{NG}) serve as the primary input power for the system and must supply the required electricity demand (L_E) and heat demand (L_H), respectively (Zidan & Gabbar, 2016). Conversion efficiency is considered and can be mathematically expressed as shown in Eq. (3.1).

$$\begin{bmatrix} L_E \\ L_H \end{bmatrix} = \begin{bmatrix} \eta_{TR} & \eta_{MT}^{E} & 0 \\ 0 & \eta_{MT}^{H} & \eta_{GB} \end{bmatrix} \begin{bmatrix} P_E \\ P_{NG}^{1} \\ P_{NG}^{2} \end{bmatrix} + \begin{bmatrix} P_{WPS}^{i} + P_{FC} \\ 0 \end{bmatrix}. \tag{3.1}$$

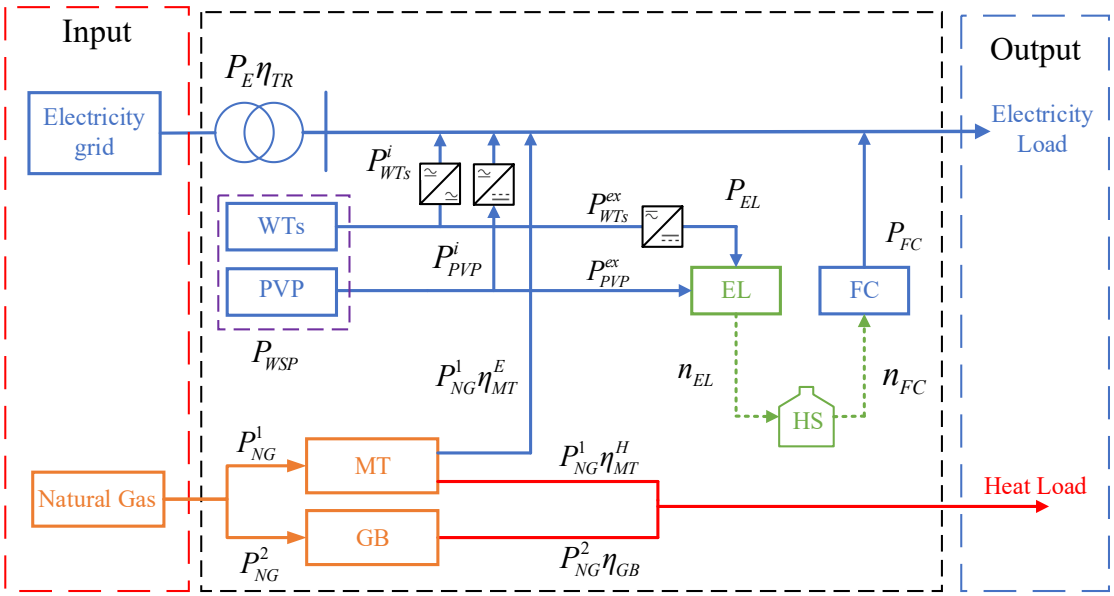

Figure 3.1 The components of MES with EH model

In part of WTs and PVPs modeling, the wind speed profile must be evaluated at a height corresponding to the turbine's cross-sectional area. Therefore, Eq. (3.2) illustrates a calculation for estimating wind speed at this altitude based on the power law theory (Manwell et al., 2002).

$$\frac{v_{WT}(h)}{v_{WT,r}(h)} = \left(\frac{z}{z_r}\right)^{\alpha}. \tag{3.2}$$

A wind turbine generates electricity when the wind speed is above the cut-in speed or below the cut-off speed, otherwise the turbine produces no power.

The power output increases with the cube of the wind speed divided by the rated wind speed when the wind speed is between the cut-in speed and the rated wind speed. Once the wind speed reaches the rated level, the turbine generates a constant rated power until the cut-off speed is reached. Above the cut-off speed condition, it is shut down to prevent damage. A wind turbine power output can be expressed Eq. (3.3) (Dechjinda & Chayakulkheeree, 2024):

$$P_{WT}(h)=\begin{cases} 0 \quad \text{for} \quad 0<v_{WT}(h)\le v_{cut-in}, \\ P_{WT,rated}\times\left(\dfrac{v_{WT}(h)}{v_{wt,rated}}\right)^3 \text{ for } v_{cut-in}<v_{WT}(h)\le v_{WT,rated}, \\ P_{WT,rated} \quad \text{for} \quad v_{WT,rated}<v_{WT}(h)\le v_{cut-off}, \\ 0 \quad \text{for} \quad v_{WT}(h)>v_{cut-off}. \end{cases} \tag{3.3}$$

The total wind power per hour from Eq. (3.3) can be defined as the sum of individual wind turbines, defined as WTs can be modeled in Eq. (3.4). The PVPs can be modeled as Eq. (3.5) which considers solar energy converted into electrical energy. The output is DC power and needs to be converted into AC power through an inverter (Yammani et al., 2012).

$$P_{WTs}(h)=\sum_{k=1}^{NT}P_{WT,k}(h), \tag{3.4}$$

$$P_{PVPs}(h)=A\times\beta\times SI(h). \tag{3.5}$$

When the wind and solar power are excessed, it can be stored in the form of hydrogen. Therefore, the grid-injected wind and solar power at time *h* can be shown in Eq. (3.6) - (3.11).

$$P_{WTs}(h)=P^{i}_{WTs}(h)+P^{ex}_{WTs}(h), \tag{3.6}$$

$$P_{PVPs}(h)=P^{i}_{PVPs}(h)+P^{ex}_{PVPs}(h), \tag{3.7}$$

$$P_{WSP}(h)=P_{WTs}(h)+P_{PVPs}(h), \tag{3.8}$$

$$P^{ex}_{WSP}(h)=\begin{cases} 0 & if\ P^{i}_{WTs}(h)+(P^{i}_{PVPs}(h)\times\eta_{DC/AC})\le L_E(h) \\ (P^{i}_{WTs}(h)+(P^{i}_{PVPs}(h)\times\eta_{DC/AC}))-L_E(h) & if\ P^{i}_{WTs}(h)+(P^{i}_{PVPs}(h)\times\eta_{DC/AC})>L_E(h) \end{cases}, \tag{3.9}$$

$$P^{i}_{WSP}(h)=\begin{cases} (P^{i}_{WTs}(h)+(P^{i}_{PVPs}(h)\times\eta_{DC/AC})) & if\ P^{i}_{WTs}(h)+(P^{i}_{PVPs}(h)\times\eta_{DC/AC})\le L_E(h) \\ L_E(h) & if\ P^{i}_{WTs}(h)+(P^{i}_{PVPs}(h)\times\eta_{DC/AC})>L_E(h) \end{cases}, \tag{3.10}$$

$$P_{EL}(h)=(P^{ex}_{WTs}(h)\times\eta_{AC/DC})+P^{ex}_{PVPs}(h). \tag{3.11}$$

The conversion devices are TR, GB, and MT. In the electrical energy sector, TR is used to convert the grid voltage to the load. The TR efficiency model can

be expressed as Eq. (3.12) when electricity flows through the TR to supply loads. In the NG energy sector, GB and MT are employed to convert NG to power (Ha et al., 2017; Thanh-tung et al., 2016). The efficiencies of the GB and MT are utilized to determine the load supply from NG formed as in Eq. (3.13) and (3.14). When considering NG cost, the power from NG can be defined as Eq. (3.15).

$$P_{TR} = P_E \eta_{TR}. \tag{3.12}$$

$$P_{GB} = P_{NG}^2 \eta_{GB}, \tag{3.13}$$

$$P_{MT}^{E,H} = \begin{cases} P_{NG}^1 \eta_{MT}^E; \text{ for electricity output} \\ P_{NG}^1 \eta_{MT}^H; \text{ for heat output} \end{cases}, \tag{3.14}$$

$$P_{NG} = P_{NG}^1 + P_{NG}^2. \tag{3.15}$$

HS has gained considerable attention in recent studies and research efforts. In these systems, hydrogen is produced by EL when the power generated by WTs and PVPs exceeds the power demand and is stored as a chemical substance. This stored hydrogen can later be used in the FC, where it reacts with oxygen from the air to generate electricity in its gaseous state. HS enables long-term energy retention, as highlighted in (Ould Amrouche et al., 2016). By applying Faraday's law, the molar flow rate of hydrogen is produced by the EL. The FC turns hydrogen into electricity, and hydrogen consumption is directly proportional to its power output (Cau et al., 2014; Imeni et al., 2023). The molar flow of EL and FC can be described as a function in Eq. (3.16) and (3.17), respectively. When HS is operating, the FC and EL cannot be operated simultaneously. Therefore, Y_{EL} and Y_{FC}, representing binary numbers (0,1), are introduced for FC and EL operating conditions as shown in Eq. (3.18) (Cau et al., 2014; Imeni et al., 2023). A key control variable in the HS system is the hydrogen tank pressure at each hour. The tank pressure reflects the amount of hydrogen contained in the storage vessels and molar flow from Eq. (3.16) and (3.17) are used to calculate the pressure at each hour. The pressure calculation for the hour *h* is dependent on the previous time step, as shown in Eq. (3.19) and can calculate the state of the tank (SOT) as shown in Eq (3.20) (Cau et al., 2014; Imeni et al., 2023).

$$n_{H_2,EL} = \frac{\eta_{EL} P_{EL}}{LHV_{H_2}}, \tag{3.16}$$

$$n_{H_2,FC} = \frac{P_{FC}}{\eta_{FC} LHV_{H_2}}. \tag{3.17}$$

$$Y_{EL} = \begin{cases} 1 \text{ when } Y_{FC} = 0 \\ 0 \text{ when } Y_{FC} = 1 \end{cases}. \tag{3.18}$$

$$p_{\text{tank}}(h) = p_{\text{tank}}(h-1) + (\frac{\Re T_{H_2}}{V_{H_2}} n_{H_2,EL}(h) - n_{H_2,FC}(h)), \tag{3.19}$$

$$SOT(h) = \frac{p_{\text{tank}}(h) - p_{\text{tank,min}}}{p_{\text{tank,rated}} - p_{\text{tank,min}}} \times 100\%. \tag{3.20}$$

3.2.2 Objective Function

The proposed method uses the PSO-LP technique to find the optimal scheduling of MES-WSPHS. The multiple energy deliveries are formed as variables on an hourly basis, to find the optimal solution for the system that makes it the minimum operating cost. The analysis considers the TOU tariff and RTP as separate factors throughout the day. Therefore, the objective function is to minimize TOC while accounting for the TOU tariff and RTP independently, with a penalty function incorporated to address any constraints violations, as shown in Eq. (3.21). The operation of this work procedure, which involves calculating the objective function while handling constraints, follows the workflow depicted in Fig. 3.2.

$$Minimize\ TOC = \sum_{h=1}^{24} (C_E(h) P_E(h) + C_{NG}(h) P_{NG}(h)) + PNF. \tag{3.21}$$

Subjected to the power balance constraints in Eq. (3.22) - (3.23),

$$L_E(h) - P_{FC}(h) - P_{WSP}^{i}(h) = P_{TR}(h) + P_{MT}^{E}(h), \tag{3.22}$$

$$L_H(h) = P_{GB}(h) + P_{MT}^{H}(h), \tag{3.23}$$

and the limit constraints of each conversion device as demonstrated by Eq. (3.24) - (3.29).

$$0 \le P_{TR}(h) \le P_{TR,rated}, \tag{3.24}$$

$$0 \le P_{MT}^{E,H}(h) \le P_{MT,rated}^{E,H}, \tag{3.25}$$

$$0 \le P_{GB}(h) \le P_{GB,rated}, \tag{3.26}$$

$$0 \le Y_{EL} P_{EL}(h) \le P_{EL,rated}, \tag{3.27}$$

$$0 \le Y_{FC} P_{FC}(h) \le P_{FC,rated}, \text{ and} \tag{3.28}$$

$$p_{\text{tank,min}} \le p_{\text{tank}}(h) \le p_{\text{tank,rated}}. \tag{3.29}$$

The initial pressure which is indicated in the content of the HS tank is set to the final pressure when the day is over, as shown in Eq. (3.29). Additionally, penalty function terms can handle some constraints, which can't define a lower and upper boundary such as Eq. (3.29) and (3.30). The penalty function can be defined in Eq. (3.31)

$$p_{\text{tank}}(h = initial) = p_{\text{tank}}(h = 24). \tag{3.30}$$

$$PNF = \rho[(p_{\text{tank}}(t) - p_{\text{tank,min}})^2 + (p_{\text{tank}}(t) - p_{\text{tank,max}})^2 + (p_{\text{tank}}(24) - p_{\text{tank}}(\text{initial}))^2] \tag{3.31}$$

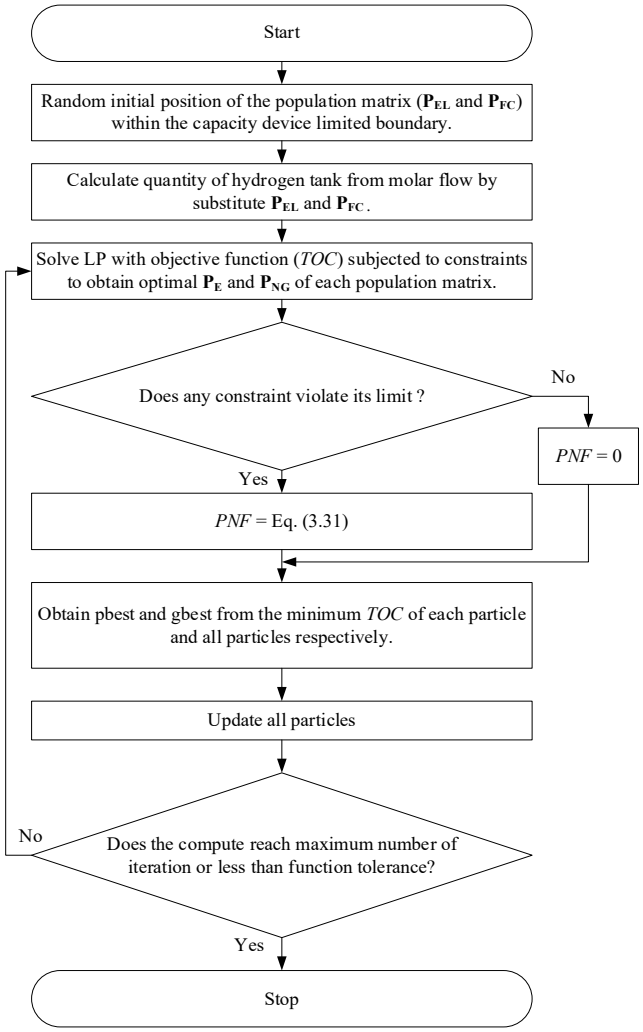

Figure 3.2 Flowchart of the PSO-LP technique under TOC procedure

3.2.3 PSO-LP Technique

The HS scheduling is a continuous variable (P_{EL} and P_{FC}), while the relation of power from the grid and NG (P_E and P_{NG}) can be formed as a linear problem. Therefore, we modify the mathematical formulation of the problem to account for utilizing a heuristic algorithm in the main loop and utilizing a deterministic algorithm in the subroutines. LP will optimize the problem in subroutines. Then, the main loop will be optimized by PSO. The overview concept of hybrid PSO-LP is shown in Fig. 3.3.

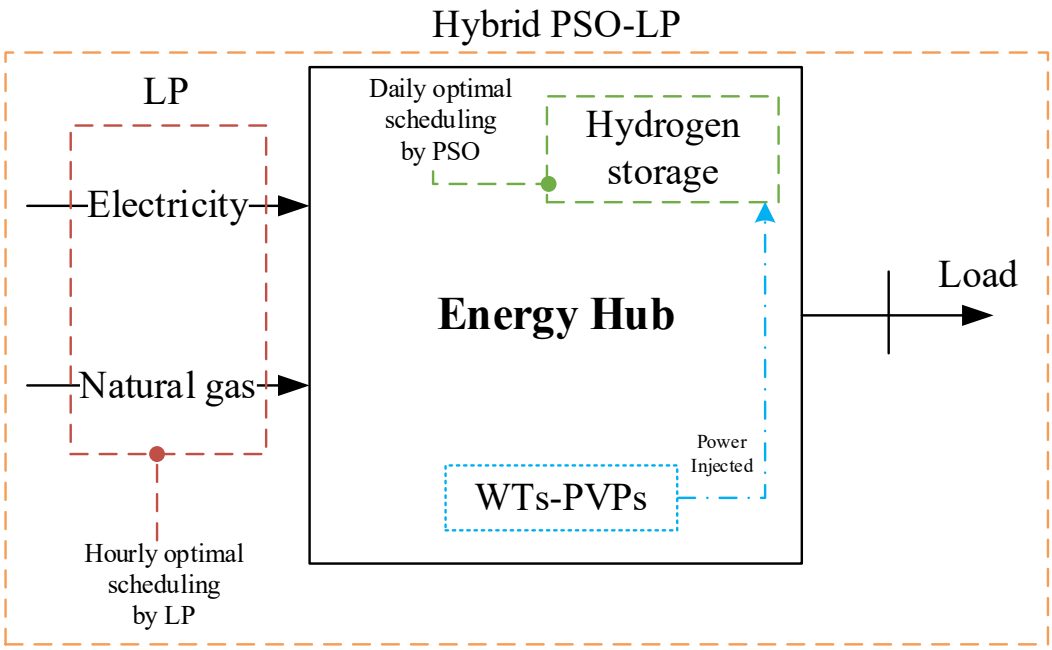

Figure 3.3 The overview of hybrid PSO-LP

The hybrid PSO-LP technique is an enhanced model of the traditional PSO algorithm, designed to be more efficient. The PSO is used for searching for optimal HS scheduling incorporating the optimal condition of electricity from the power grid and NG, under wind and solar power, electricity load, and heating load conditions. As a stochastic optimization technique, the PSO algorithm is a stochastic optimization technique inspired by the collective behavior of bird flocks and their emergent dynamics. In PSO, a population of potential solutions, referred to as particles, is used to search for the optimal result. This population is called a swarm, and each particle

represents a possible solution. The algorithm begins by randomly assigning positions to the particles within the search space. These particles then update their positions in successive iterations, adjusting based on their velocities. Each particle keeps track of its best position, referred to as *pbest(i,h)*, and updates its velocity based on that. Particles also communicate with one another to adjust their movement. If a particle finds a solution better than its previous *pbest*, the value is replaced. Among the entire population, the best solution found is called the global best (*gbest*). In this work, the population is formulated as follows Eq. (3.32) and the matrix in Eq. (3.32) will solve the individual objective function simultaneously. Then this matrix is used to update each particle's velocity as displayed in Eq. (3.33), and the next step of the matrix is updated by velocity as shown in Eq. (3.34) (Kennedy & Eberhart, 1995).

$$\mathbf{P_{EL,FC}} = [P_{EL,FC}(1), P_{EL,FC}(2), ..., P_{EL,FC}(h), ..., P_{EL,FC}(24)]. \quad (3.32)$$

$$v(i,h+1) = wv(i,h) + c_1 rand_1(pbest(i,h) - \mathbf{P_{EL,FC}}(i,h)) + c_2 rand_2(gbest(i,h) - \mathbf{P_{EL,FC}}(i,h)), \quad (3.33)$$

$$\mathbf{P_{EL,FC}}(i,h+1) = \mathbf{P_{EL,FC}}(i,h) + v(i,h+1). \quad (3.34)$$

In this work, Eq. (3.32) defines the upper and lower boundaries based on the operational range of energy converter components in Table 3.1, specifically from 0 to $P_{EL,rated}$ and 0 to $P_{FC,rated}$. In cases where the excess power from RE is less than the rated capacity of the EL, the upper boundary is redefined by Eq. (3.11).

Although PSO is effective in exploring global search spaces, it often encounters challenges in fine-tuning solutions within constrained environments due to its stochastic nature. To overcome this limitation, the LP algorithm is incorporated into the proposed PSO-LP framework. After PSO generates an initial HS scheduling solution, LP is employed to further refine and optimize the solution under a set of linear constraints and objective functions. By combining the global exploration capability of PSO with the local optimization precision of LP, the hybrid approach aims to achieve faster convergence, improved solution accuracy, and enhanced feasibility for multi-energy system scheduling problems. The mathematical formulation of the LP optimization stage is established as follows and can be expressed by Eqs. (3.35)–(3.41).

$$\text{minimize } TOC = \mathbf{C}^{\mathbf{T}}\mathbf{x} \tag{3.35}$$

$$\mathbf{C} = [C_{E_{(24\times1)}}; C_{NG_{(24\times1)}}; C_{NG_{(24\times1)}}] \in \mathbb{R}^{72\times1} \tag{3.36}$$

$$\mathbf{x} = [P_{E_{(24\times1)}}; P^{1}_{NG_{(24\times1)}}; P^{2}_{NG_{(24\times1)}}] \in \mathbb{R}^{72\times1} \tag{3.37}$$

Subject to $\mathbf{A_{eq}}\mathbf{x} = \mathbf{b_{eq}}$ (3.38)

$$lb \le \mathbf{x} \le ub \tag{3.39}$$

$$\mathbf{A_{eq}} = \begin{bmatrix} \mathbf{A}_{11} & \mathbf{A}_{12} & \mathbf{0}_{(24\times24)} \\ \mathbf{0}_{(24\times24)} & \mathbf{A}_{22} & \mathbf{A}_{23} \end{bmatrix} \in \mathbb{R}^{48\times72} \tag{3.40}$$

$$\mathbf{b_{eq}} = \left[L_E(h)_{(1\times24)}, L_H(h)_{(1\times24)} \right]^T \tag{3.41}$$

Where

$$\mathbf{A_{11}} = diag(\eta_{TR}) \in \mathbb{R}^{24\times24}$$

$$\mathbf{A_{12}} = diag(\eta^{E}_{MT}) \in \mathbb{R}^{24\times24}$$

$$\mathbf{A_{22}} = diag(\eta^{H}_{MT}) \in \mathbb{R}^{24\times24}$$

$$\mathbf{A_{23}} = diag(\eta_{GB}) \in \mathbb{R}^{24\times24}$$

$\mathbf{0}_{(24\times24)}$ = zero matrix (no coupling)

The matrices denoted as *diag(·)* represent diagonal matrices, where all off-diagonal elements are equal to zero. Each diagonal entry corresponds to a parameter specific to a given time step or energy source. Furthermore, the optimization problem is subject to lower and upper bounds, denoted as *lb* and *ub*, respectively. The lower bound is always set to zero, while the upper bound is defined based on the energy flow pathways through the system. Specifically, the upper bound is assigned according to the rated capacity of each device along its respective energy flow path, as detailed in Table 3.1.

3.3 Data Acquired and Assumptions

To evaluate the performance and feasibility of the MES-WSPHS configuration, it is essential to analyze the efficiency and capabilities of its individual components as shown in Table 3.1 (Ha et al., 2022; Son et al., 2021). The electricity load profile utilized in this study is obtained from a typical summer day in the northeastern region of Thailand, with a peak load defined at 2 MW (Dechjinda & Chayakulkheeree, 2024) as shown in Fig. 3.4(a). The heat load profile is adapted from Anna Sandhaas as illustrated

in Fig. 3.4(b). The wind and solar profile are derived from data collected on a summer day in Pakchong, Thailand (Dechjinda & Chayakulkheeree, 2024). Finally, additional details of the entire energy profile are provided in Appendix A.

Table 3.1 The efficiency and rated device of each component

List	No.1	No.2	No.3	No.4	No.5	No.6	No.7
Component	TR	EL	FC	MT	GB	Converter	Pressure tank
Efficiency	98%	70%	60%	40%, 50%	88%	95%	-
Rated	2500 kVA	500 kW	500 kW	500 kW	1600 kW	-	100 bar

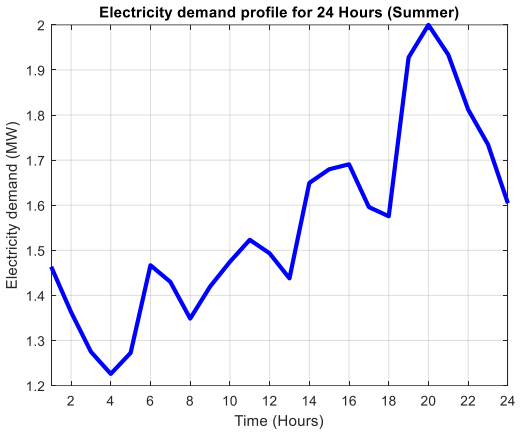

(a)

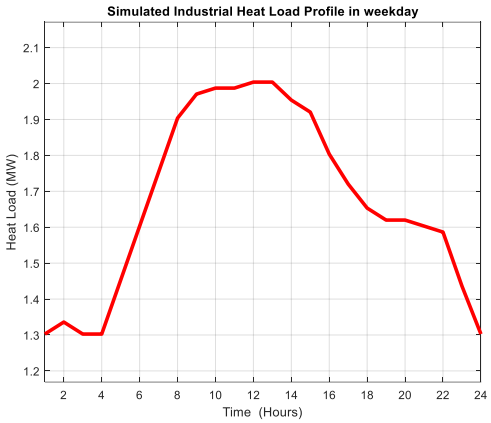

(b)

Figure 3.4 The load profile (a) electricity (b) heat

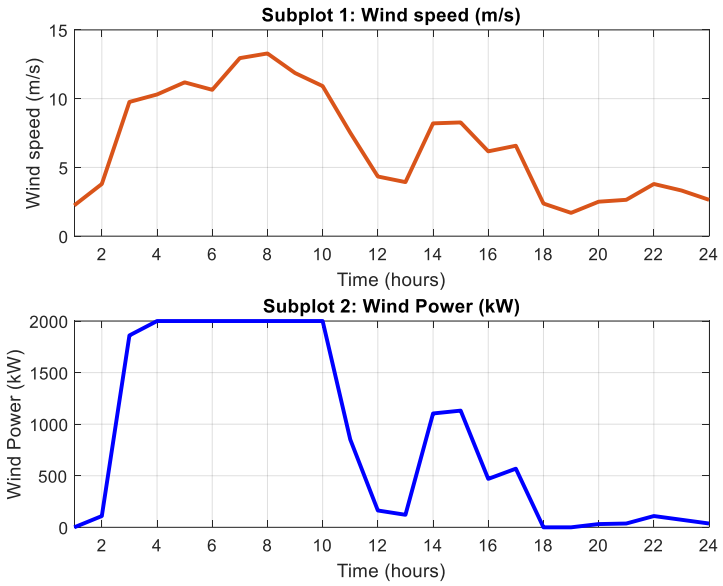

Figure 3.5 The wind profile

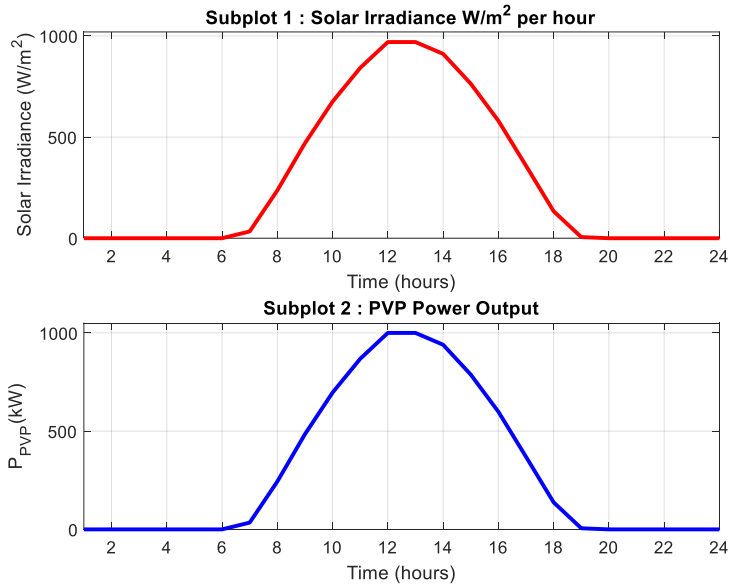

Figure 3.6 The solar profile

This study examines a wind power system with four turbines rated at 500 kW each (NT = 4), as shown in Fig. 3.5. Subplots 1 and 2 in Fig. 3.5 illustrate wind speed conversion to power. Hourly solar irradiance and PVPs output are shown in Fig. 3.6, subplots 1 and 2, respectively. Fig. 3.7 highlights excess wind and solar power over

demand. Electricity costs follow TOU tariff (Piawises & Chayakulkheeree, 2024), while NG prices remain constant. Furthermore, RTP, which reflects dynamic price adjustments, both are described in Fig. 3.8.

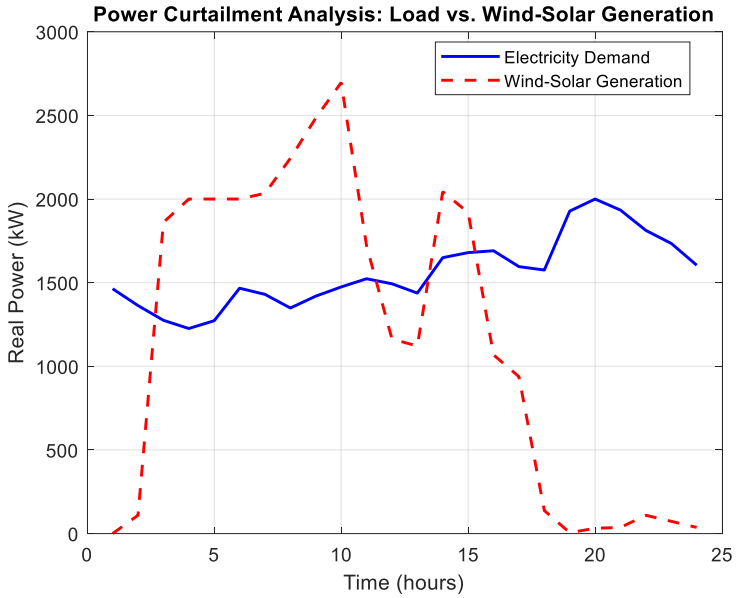

Figure 3.7 The excess wind-solar generation

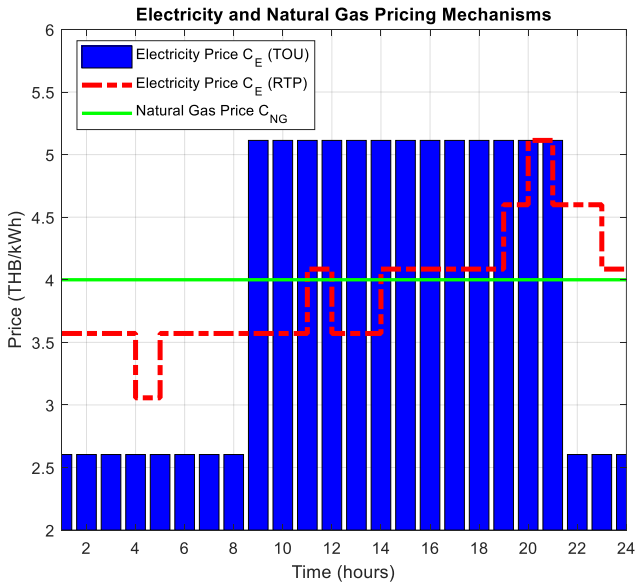

Figure 3.8 The electricity and natural gas pricing mechanism

3.4 Simulation Results

The case studies presented in Fig. 3.9 are analyzed under five distinct scenarios, each with specific operational conditions:

Case I: MES-WSP operates without HS and lacks coordination between electricity and NG (Base Case).

Case II: MES-WSP includes HS with no coordination between electricity and NG.

Case III: MES-WSP operates with coordinated electricity and NG but without HS.

Case IV: MES-WSP (excluding solar power) operates with HS and coordinated electricity and NG operations.

Case V: MES-WSP operates with HS and coordinated electricity and NG operations.

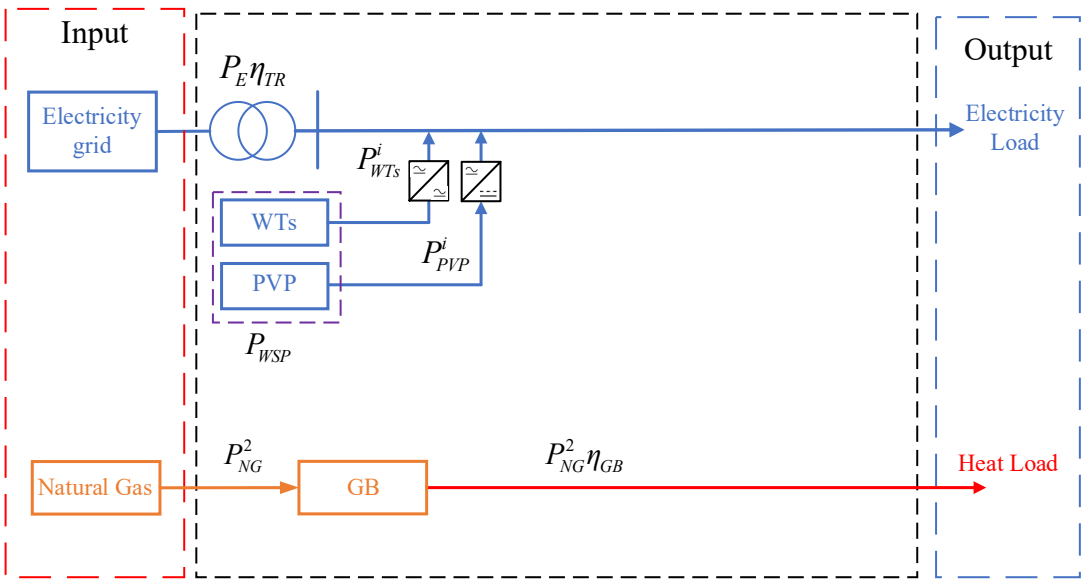

(a)

Figure 3.9 Configuration of the MES-WSP under different case studies

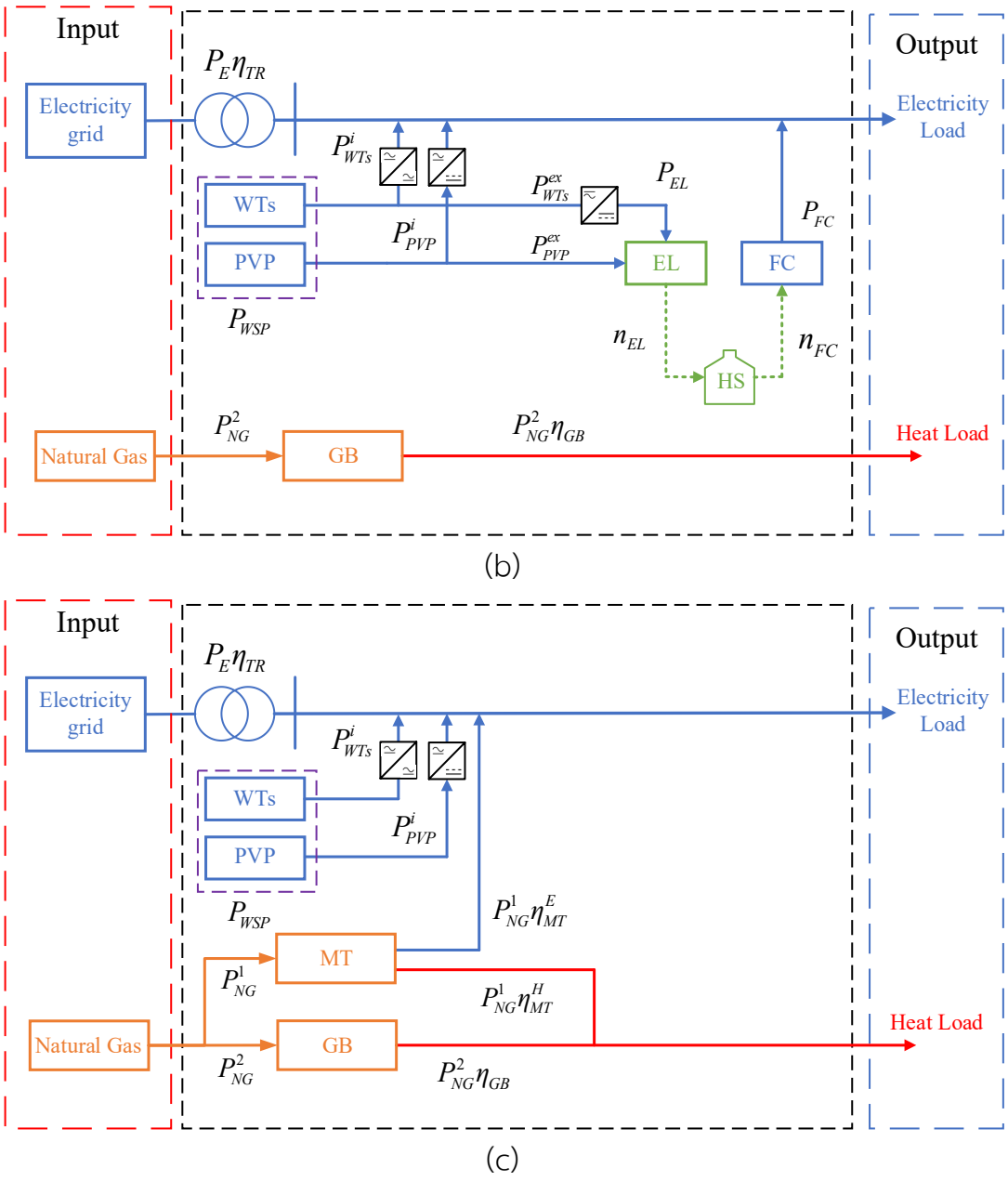

Figure 3.9 Configuration of the MES-WSP under different case studies (Continued)

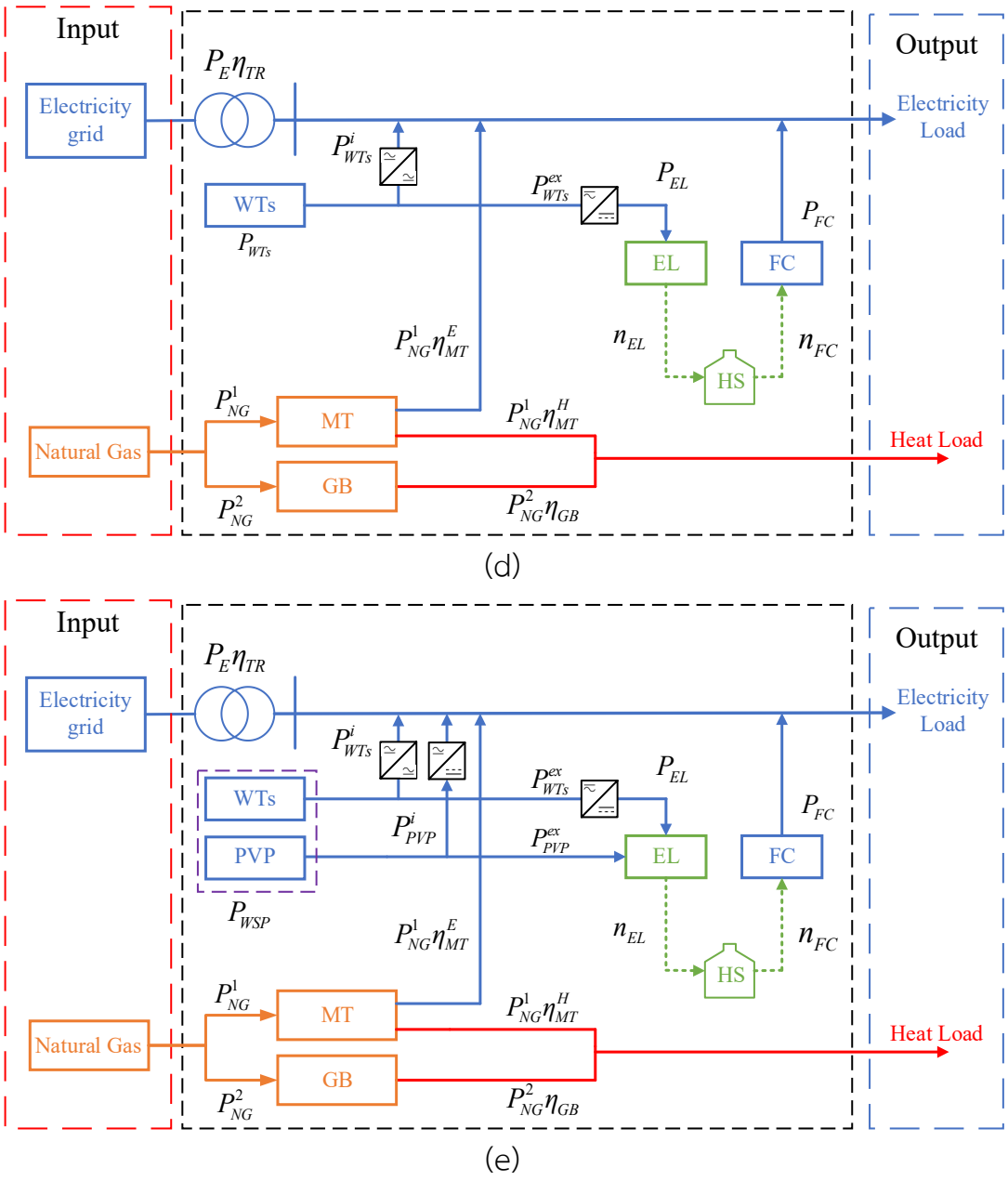

Figure 3.9 Configuration of the MES-WSP under different case studies (Continued)

However, the case studies will be analyzed under the TOU scheme for all given cases, while under the RTP scheme, only the case with the lowest TOC will be considered and presented. This analysis aims to determine which scenario achieves the greatest reduction in operating costs throughout the day.

3.4.1 Optimization Parameter Validation

To determine the optimal solution for minimizing the TOC considering Case IV, a sensitivity analysis is conducted on the PSO-LP method. The analysis involved varying key PSO parameters, specifically the inertia weight (w) and cognitive and learning factors (c_1, c_2), to assess their impact on optimization performance. Specifically, an adaptive inertia weight is used while varying the cognitive and learning factors. Conversely, the cognitive and learning factors are kept at their default values while varying inertia weight. These parameters can be modeled as shown in Table 3.2.

Table 3.2 Vary the parameters w, c1, and c2 of the PSO-LP settings

Variable	Settings							
	Varies w			*Varies* c_1 *and* c_2				
w	0.1	0.6	1.1	[0.1,1.1]				
c_1	1.49			1.49	1	2	1	2
c_2	1.49			1.49	2	1	1	2
Random values ($rand_1, rand_2$)	[0,1]							

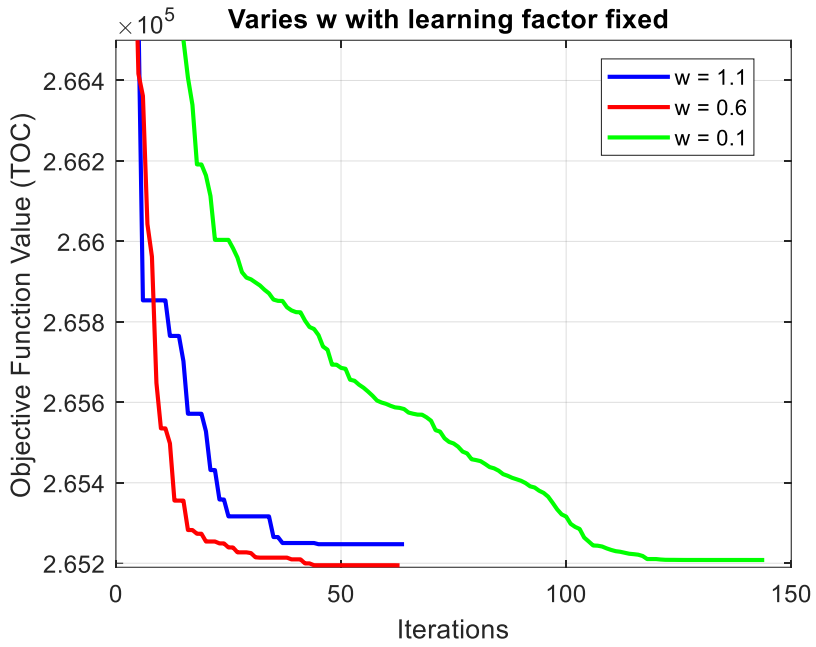

Figure 3.10 Convergence of TOC optimization with different inertia weights

The inertia weight (w) is tested at three different levels while keeping the learning factors (c_1 and c_2) constant:

- Low (w = 0.1): The best objective function value obtained is 265,208 THB.
- Medium (w = 0.6): The best objective function value obtained is 265,195 THB.
- High (w = 1.1): The best objective function value obtained is 265,247 THB.

These results suggest that an intermediate inertia weight (w = 0.6) provides better convergence performance compared to lower or higher values. The convergence plot of the variation of the inertia weight is illustrated in Fig. 3.10.

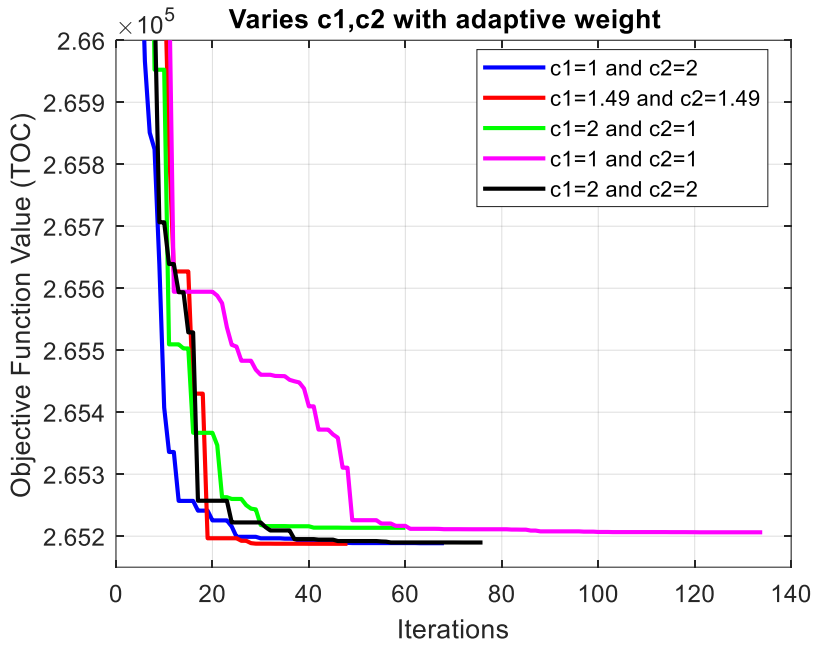

Figure 3.11 Convergence of TOC optimization with different learning factors

The cognitive and social learning factors are tested under different configurations while maintaining a fixed range of inertia weight.

- $c_1 < c_2$ ($c_1 = 1$, $c_2 = 2$):

  The best objective function value obtained is 265,189 THB.

- $c_1 = c_2$:

  - ($c_1 = 1.49$, $c_2 = 1.49$):

    The best objective function value obtained is 265,188 THB.

  - ($c_1 = 1$, $c_2 = 1$):

    The best objective function value obtained is 265,190 THB.

  - ($c_1 = 2$, $c_2 = 2$):

    The best objective function value obtained is 265,767 THB.

- $c_1 > c_2$ ($c_1 = 2$, $c_2 = 1$):

  The best objective function value obtained is 265,214 THB.

Among these settings, the combination of $c_1 = 1.49$, $c_2 = 1.49$ demonstrated the best optimization performance, yielding the lowest TOC. The

convergence plot of the variation of cognitive and social learning factors is illustrated in Fig. 3.11.

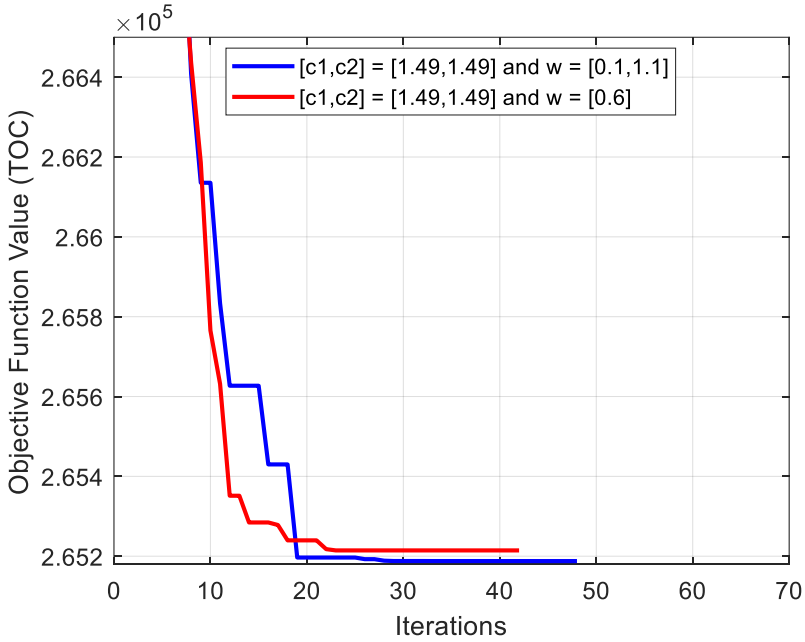

Figure 3.12 Convergence of TOC optimization with selected PSO parameters

To further refining the parameter selection, two configurations are compared from selection PSO parameters by Fig. 3.10 and Fig. 3.11 The convergence plot of the selection PSO parameters is illustrated in Fig. 3.12:

- (c_1, c_2) = (1.49, 1.49) and w = 0.6:

  The best objective function value obtained is 265,195 THB.
- (c_1, c_2) = (1.49, 1.49) and w = [0.1,1.1]:

  The best objective function value obtained is 265,188 THB.

3.4.2 TOU Tariffs Considerations

In each case, the scheduling of energy proportions varies depending on the scenario. For cases without HS, only LP is employed to find the solution since there are no variables for the FC and EL. However, in scenarios incorporating HS, a hybrid PSO-LP method is utilized. This approach first optimizes the operation of the

fuel cell and EL using PSO, and the results are subsequently processed using LP. The scheduled energy output for each component, as well as the costs associated with each energy sector, are summarized in Table 3.3. Furthermore, since HS is considered in Cases II, Case IV, and Case V, with PSO-LP employed to derive the solutions, Figs. 3.13 to 3.18 provide detailed insights into the power balance, optimization algorithm, and the impact of HS on the proposed system. The figures are organized based on case studies: (a) Case II, (b) Case IV, and (c) Case V, illustrating the effectiveness of the proposed optimization approach in achieving optimal solutions. These cases highlight the role of HS integration, both with and without the coordinated operation of NG-electricity, in balancing multiple energy types with energy demand. Notably, Case IV excludes solar power to analyze the influence of wind power injections exclusively. Furthermore, when the MT is integrated, additional power losses occur due to operational efficiency limitations. However, despite these losses, MT integration significantly contributes to reducing the TOC.

Various energy sources are utilized to meet output demands through multiple energy scheduling in the EH. In Table 3.3, Case I represents no cooperation between electricity and NG systems, where each sector operates independently, focusing solely on its efficiency. Conversely, Case III involves coordinated operation between electricity and NG, with NG being used to dispatch the electricity load via MT to reduce electricity consumption. Excess wind and solar power, as shown in Fig. 3.7, are not utilized, resulting in no additional energy savings.

Case II integrates HS without coordination with the electricity and NG systems, whereas Cases IV and Case V incorporate both HS and coordinated operation. This significantly enhances energy management strategy since HS stores only excess wind in Case IV and excess wind and solar energy in Case II and V, which is then discharged at other times. The power balance in each energy sector is depicted in Fig. 3.13(a), 3.13(b), and 3.13(c) for electricity and in Fig. 3.14(a), 3.14(b), and 3.14(c) for heat. Both Figs 3.13 and 3.14 focus exclusively on cases involving HS integration.

Table 3.3 Summary of power scheduling and energy costs for each sector

Case	Energy scheduling (kWh)										Operation costs (THB)		
	Energy through components						Demand-side				Electricity	NG	Total
	TR	MT	WTs	PVPs	FC	GB	Gen	Used	Loss	Curtailed			
I	16,956	-	20,669	7,166	-	40,130	90,382	77,530	5,818	7,034	68,887	182,410	251,297
II	15,024	-			1,933		84,996		5,779	1,687	61,711	182,410	244,121
III	15,356	3,600			-	38,130	90,679		5,913	7,236	60,538	189,319	249,857
IV	17,798	4,950		-	1,680	37,380	84,242		6,011	701	73,278	191,910	265,188
V	13,424	3,600		12,113	1,933	38,130	85,090		5,873	1,687	50,453	189,319	239,772

The energy flow through the MT, which operates in Cases III and V, produces both electricity and heat. In these cases, the MT is scheduled to run from 12 a.m. to 9 p.m., as NG costs during this period are lower than the peak electricity costs in TOU tariffs. However, when energy generation is sufficient to meet demand, the MT remains inactive, as shown in Figs. 3.13(c) and 3.14(c), where it does not operate at 2 p.m. and 3 p.m. In Case IV, where only excess wind power is utilized, the MT operates for an extended period of 11 hours from 11 a.m. to 10 p.m., resulting in the highest power loss among all cases, as indicated in Table 3.3 and shown in Figs. 3.13(b) and 3.14(b).

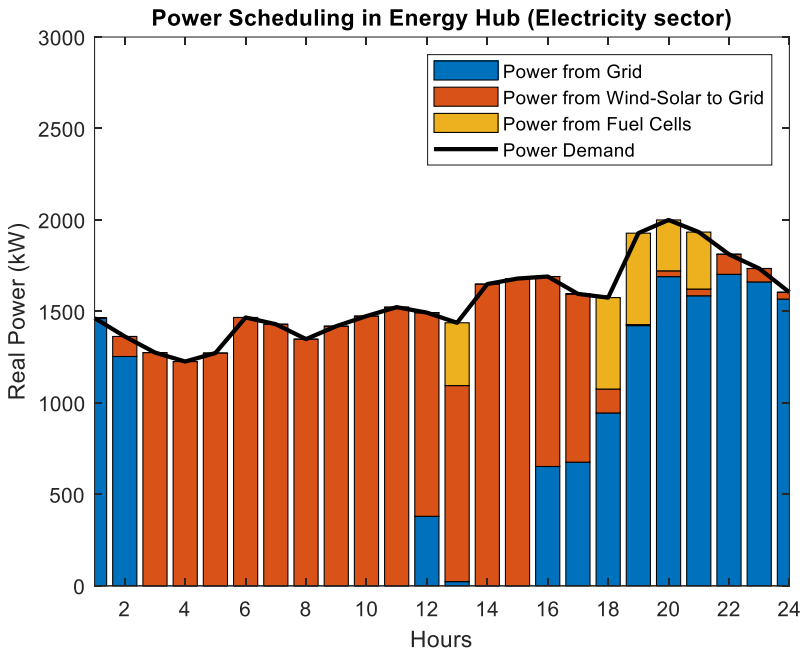

(a)

Figure 3.13 Power scheduling in EH for (a) Case II, (b) Case IV, and (c) Case V (electricity sector)

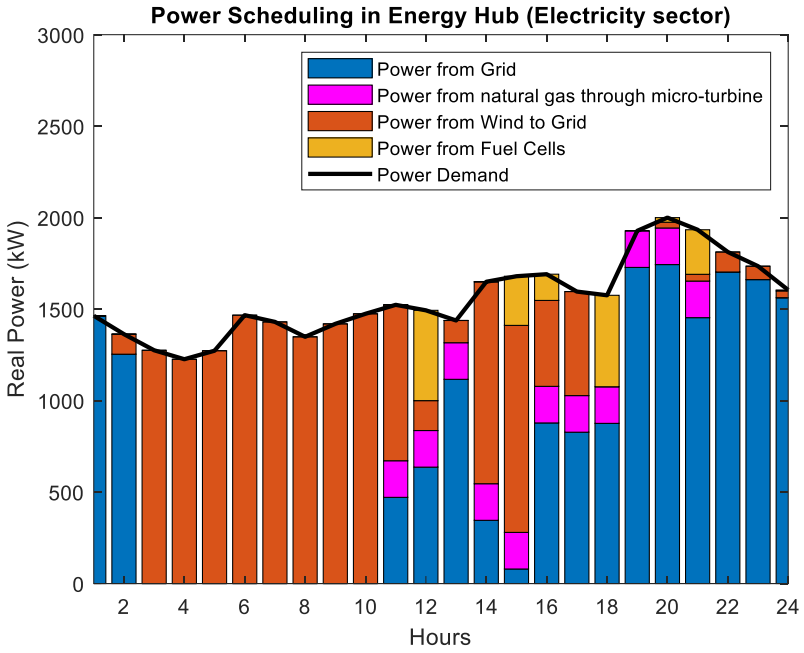

(b)

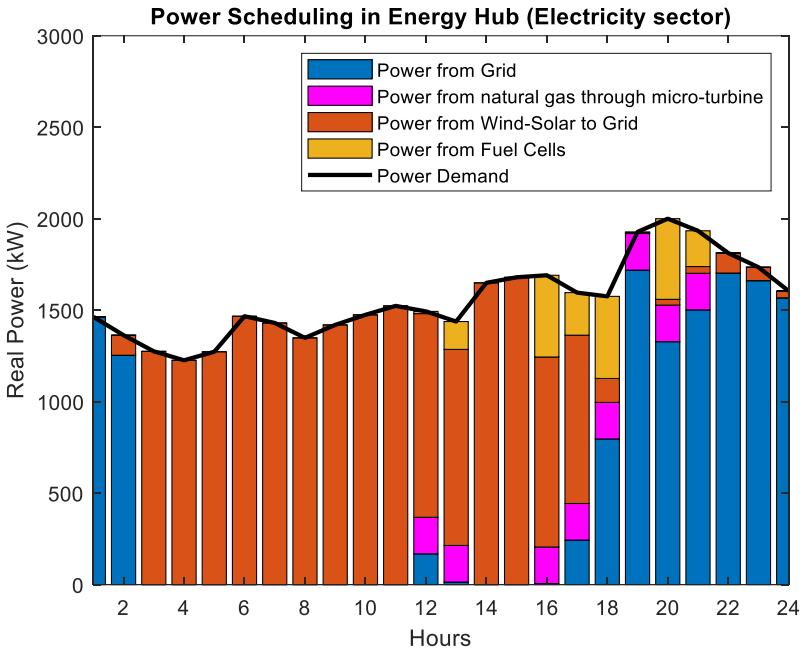

(c)

Figure 3.13 Power scheduling in EH for (a) Case II, (b) Case IV, and (c) Case V (electricity sector) (Continued)

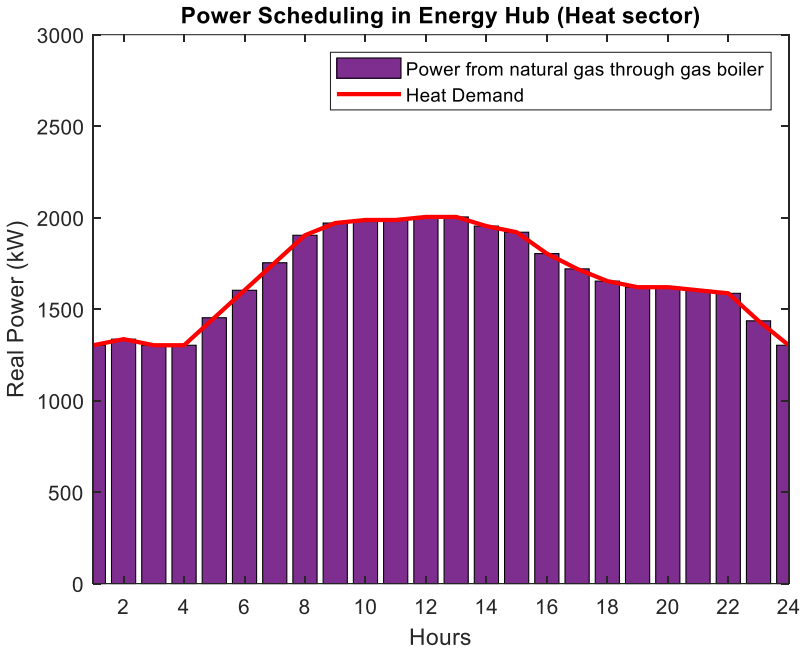

(a)

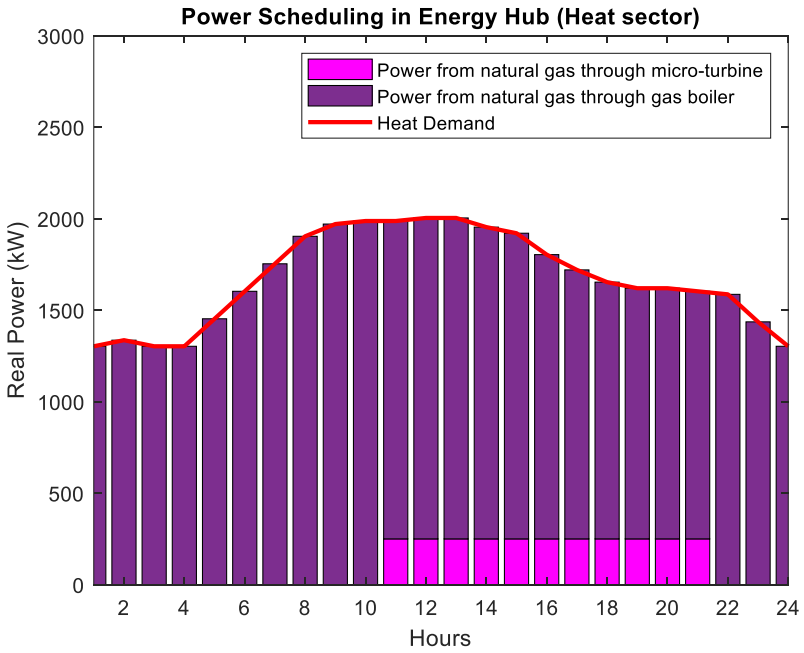

(b)

Figure 3.14 Power scheduling in EH for (a) Case II, (b) Case IV, and (c) Case V (heat sector)

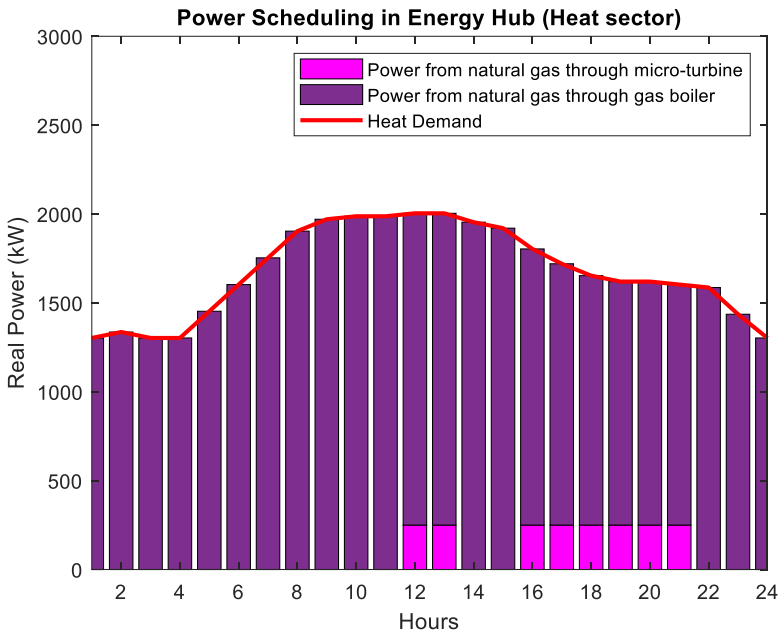

(c)

Figure 3.14 Power scheduling in EH for (a) Case II, (b) Case IV, and (c) Case V (heat sector) (Continued)

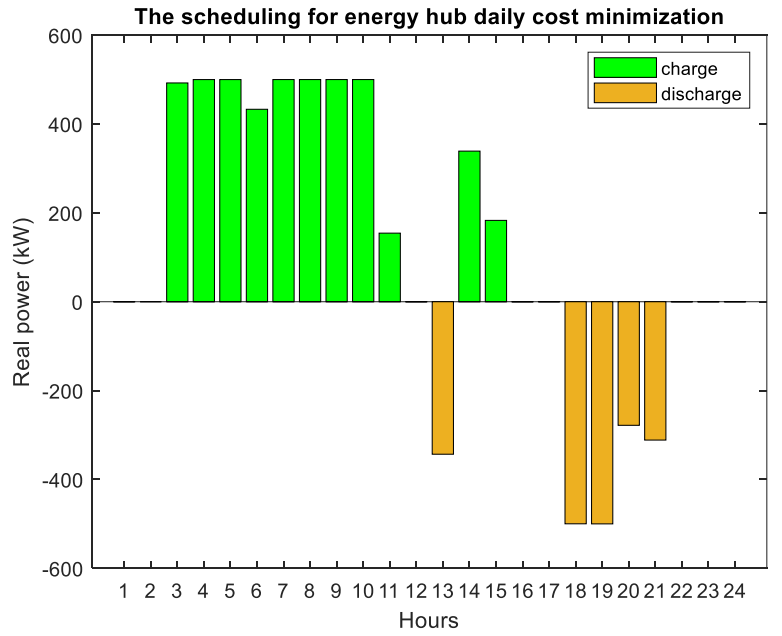

(a)

Figure 3.15 HS scheduling for 24 hours (a) Case II, (b) Case IV, and (c) Case V

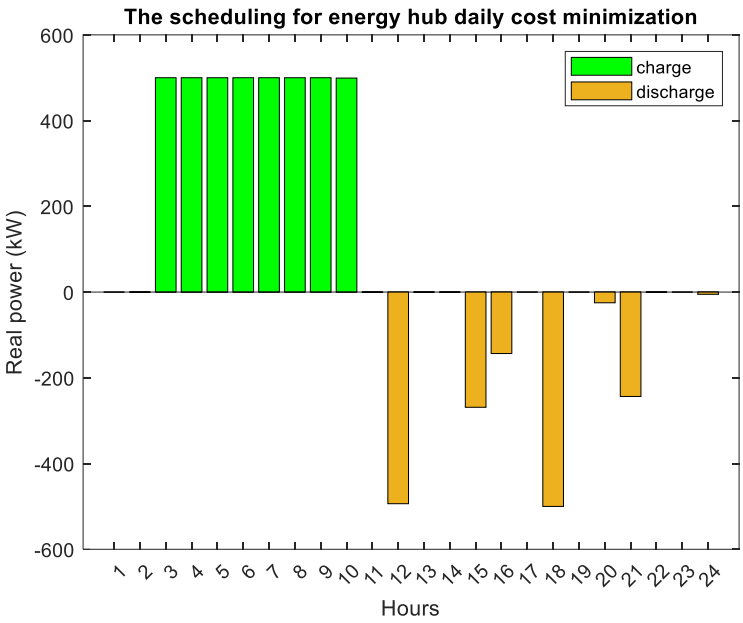

(b)

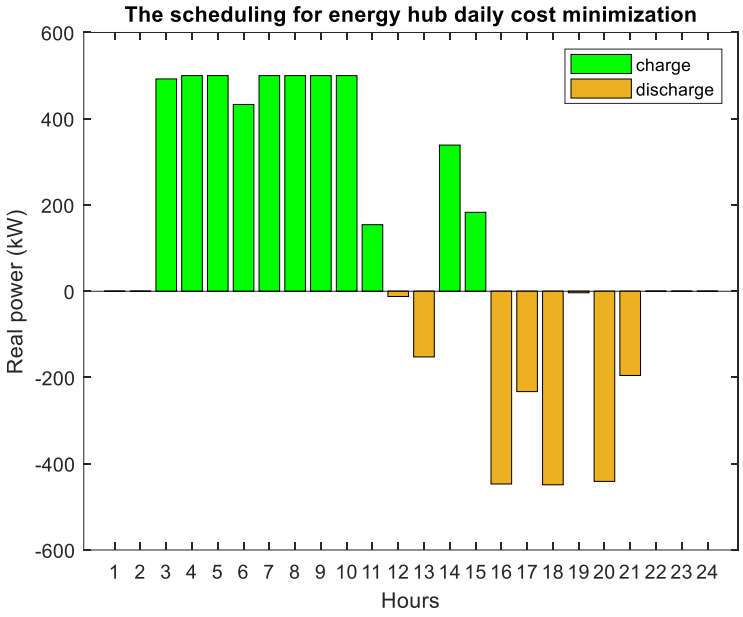

(c)

Figure 3.15 HS scheduling for 24 hours (a) Case II, (b) Case IV, and (c) Case V (Continued)

In Case II and Case V, with HS integration, EL converts excess wind and solar power into HS from 3 a.m. to 11 a.m. and 2 p.m. to 3 p.m. However, in Case IV,

due to the absence of solar energy, the EL only utilizes excess wind power for HS from 3 a.m. to 11 a.m. In all cases, FC converts stored hydrogen into electricity to reduce grid dependency, with the HS operation schedule varying across cases. Additionally, the FC scheduling patterns differ among Case II, Case IV, and Case V. However, the power from FC operated is performing in the peak electricity costs period to reduce energy from the grid, resulting in a lower TOC and energy curtailment. The TOU tariff is utilized to define the objective, resulting in the FC operating as illustrated in Fig. 3.15 (a) Case II, (b) Case IV, and (c) Case V. In the study, the initial hydrogen tank pressure is set at 20 bar. During HS scheduling, the tank pressure is maintained within a range of no more than 100 bar and no less than 10 bar, which is defined in SOT is 100% and 0%, respectively. With the pressure at the final hour of the day equal to that of the initial hour. As shown in Fig. 3.16 (a) Case II, (b) Case IV, and (c) Case V, SOT is displayed as a percentage, representing the HS model. However, further initial settings of pressure are studied in Appendix C

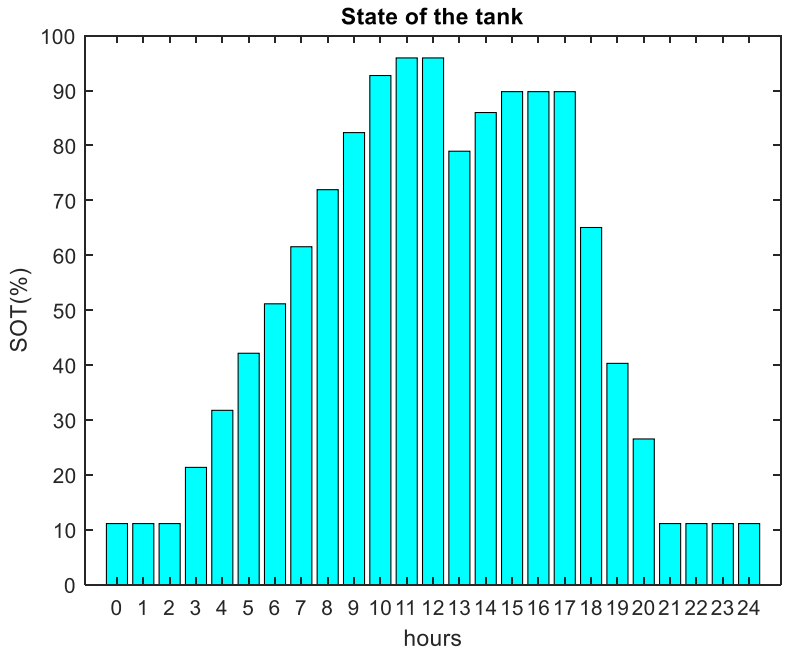

(a)

Figure 3.16 State of the tank (%SOT) in HS (a) Case II, (b) Case IV, and (c) Case V

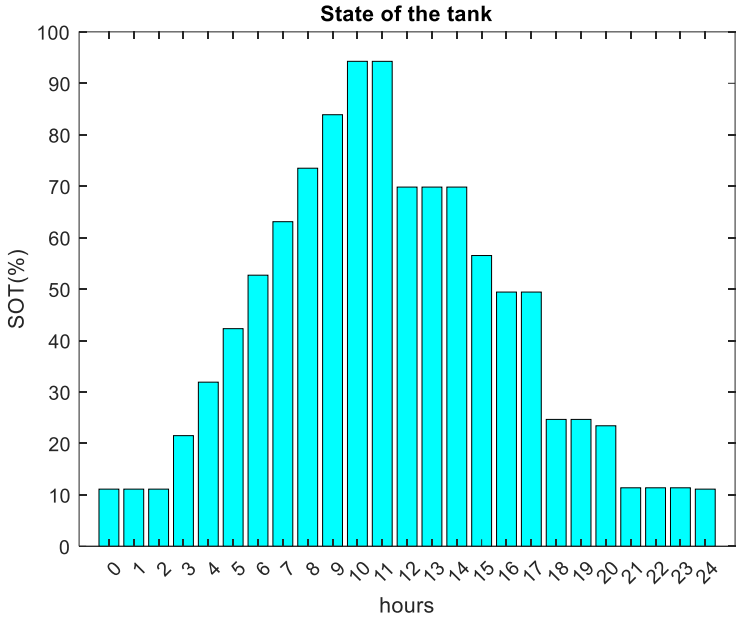

(b)

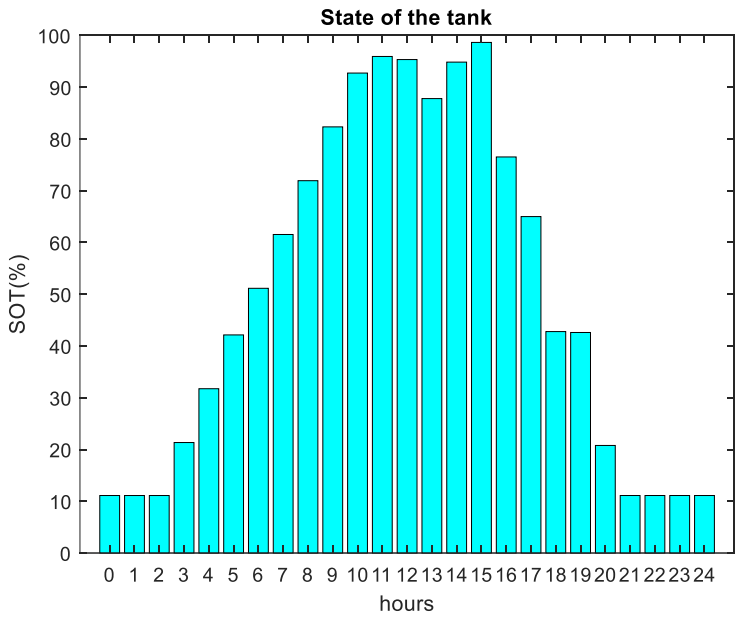

(c)

Figure 3.16 State of the tank (%SOT) in HS (a) Case II, (b) Case IV, and (c) Case V (Continued)

Figure 3.17 (a), (b) and (c) show the convergent PSO-LP solutions of Case II, Case IV, and Case V respectively. The best function value is TOC in all three cases.

Case II begins converging around 20 iterations and stops finding the optimal solution in 128 iterations. Case IV starts converging around 20 iterations and stops finding the optimal solution in 48 iterations. Case V also begins converging around 30 iterations and stops finding the optimal solution in 285 iterations. However, all cases can converge before the maximum iteration setting because the final solution is less than the function tolerance. Notably, Case IV exhibits a significant reduction in the number of iterations required to find a solution due to the stable wind speed profile during exceed hours, which operates at the rated power. As a result, Case IV is the fastest to converge.

Figure 3.18 (a) and (b) demonstrate the results from 30 trials of Case II, Case IV, and Case V which show the best, worst, and average lines of solutions, indicate that the fitness results of PSO-LP are clustered, with the standard derivations (SD) of 4.30, 3.9, and 5.11, respectively. Therefore, the proposed method is demonstrated to be reliable and has the potential to find the optimal solutions

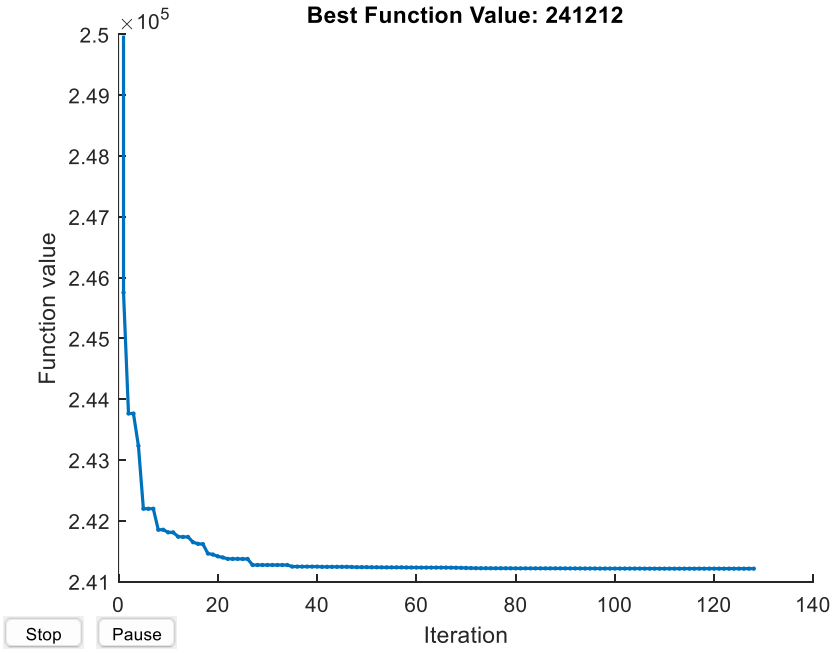

(a)

Figure 3.17 The PSO-LP convergence plot (a) Case II, (b) Case IV, and (c) Case V

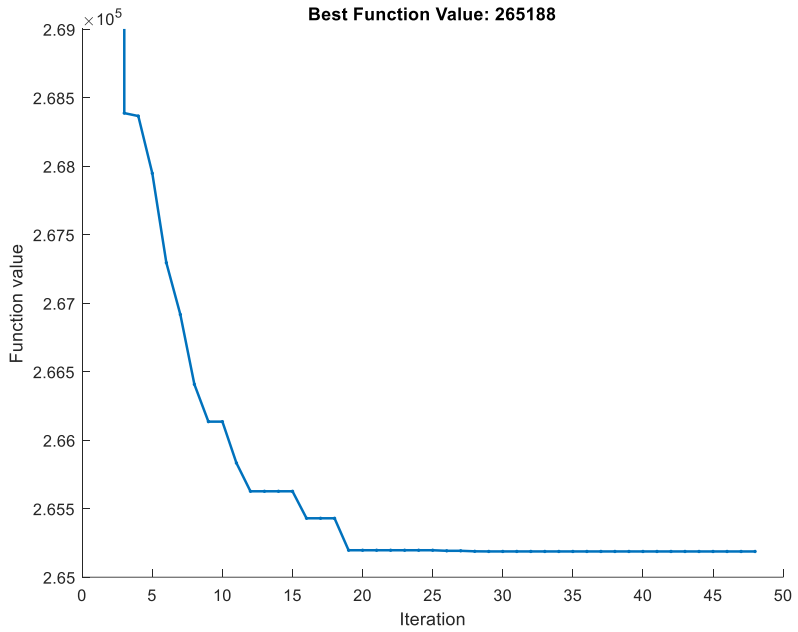

(b)

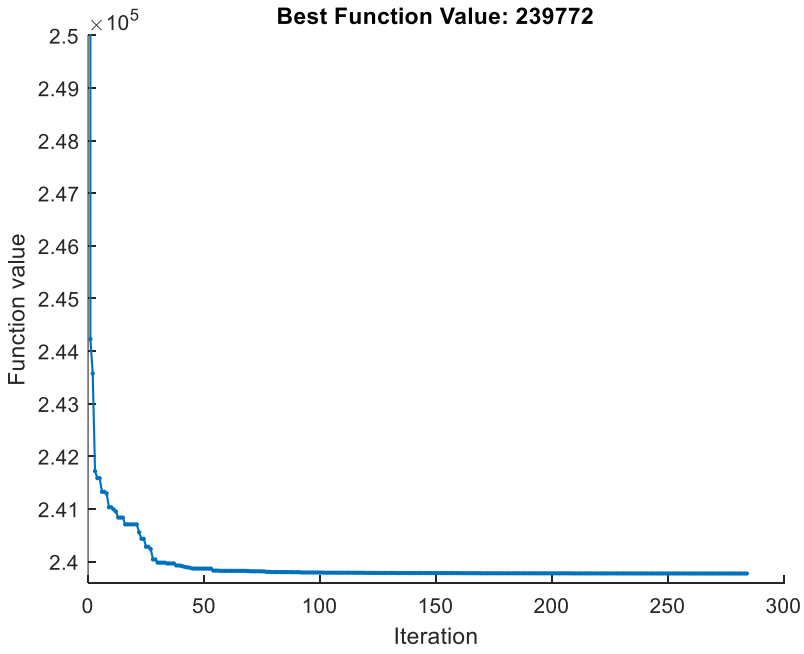

(c)

Figure 3.17 The PSO-LP convergence plot (a) Case II, (b) Case IV, and (c) Case V (Continued)

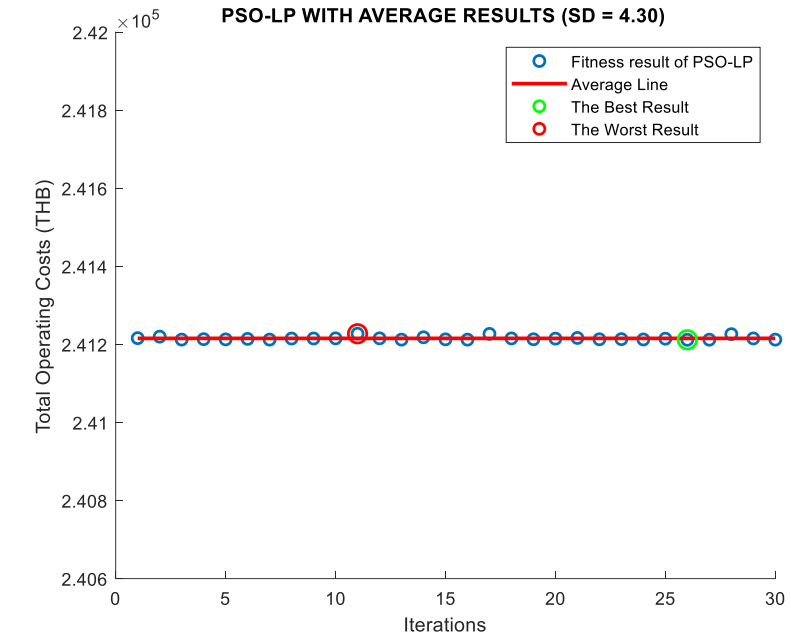

(a)

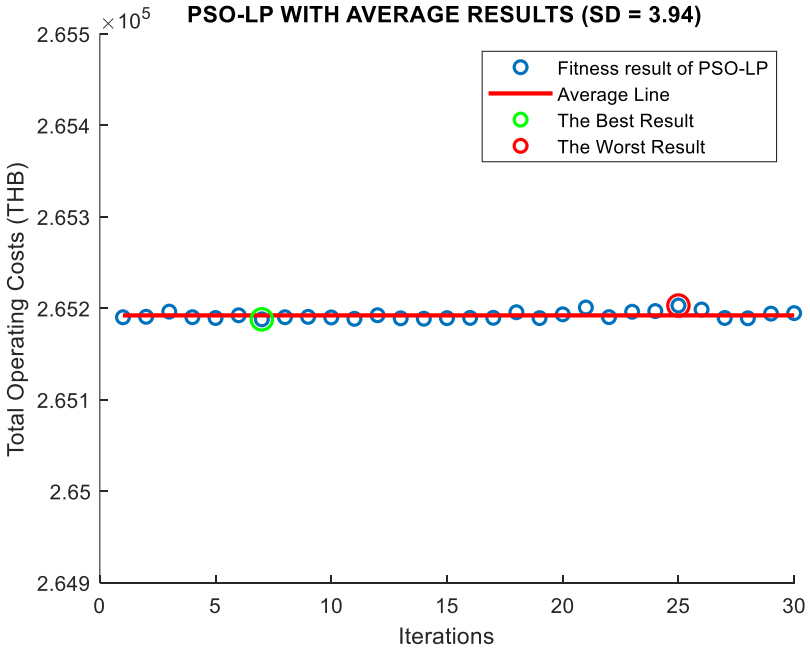

(b)

Figure 3.18 The PSO-LP fitness results with 30 iterations (a) Case II, (b) Case IV, and (c) Case V

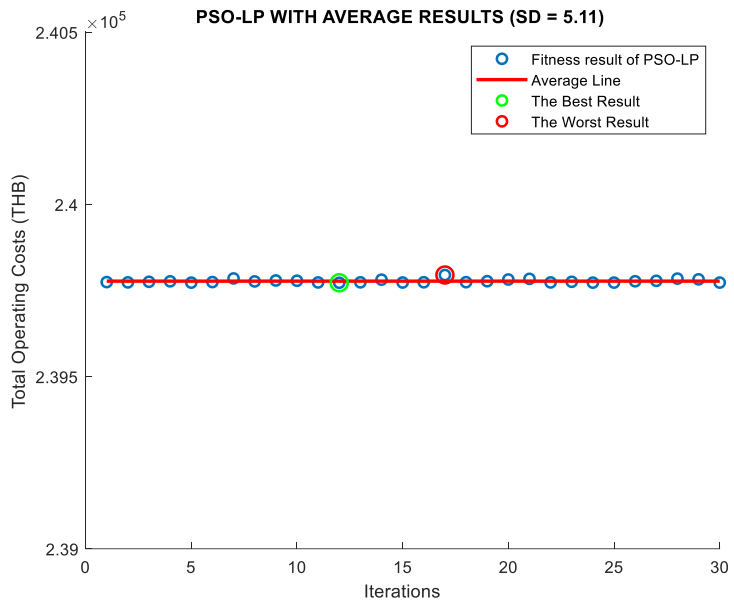

(c)

Figure 3.18 The PSO-LP fitness results with 30 iterations (a) Case II, (b) Case IV, and (c) Case V (Continued)

When comparing the results across the five case studies, TOC shows a significant reduction in all optimized scenarios compared to the base case (Case I), except for Case IV. The higher TOC in Case IV is primarily due to the limited RE profile, which excludes solar power and consequently reduces the utilization of HS. This emphasizes the effectiveness of incorporating multi-energy scheduling and single-objective optimization strategies in enhancing system cost reduction. Table 3.4 presents the TOC values for each case along with the corresponding percentage reduction relative to the base case.

Table 3.4 TOC percentage comparison across all case studies

Case study	Case I	Case II	Case III	Case IV	Case V
TOC	251,297	244,121	249,857	265,188	239,772
% Reduction from Case I	-	2.86%	0.57%	–5.53%	4.58%

3.4.3 RTP Considerations

In this section, the impact of RTP on the operation of the MES-WSPHS, which is on Case V, is analyzed. The study investigates how dynamic electricity pricing influences the scheduling of various energy resources, ensuring cost-effective and efficient energy management. Fig. 3.19 and Fig. 3.20 illustrate the power scheduling for each energy sector. In the electricity sector, MT and HS are scheduled to operate between 7 p.m. and 10 p.m., that reflects the RTP scheme indicates higher electricity prices during this period. Therefore, the power from NG through MT is occurring in both energy sectors.

The integration of HS further enhances system flexibility, as depicted in Fig. 3.21(a), which illustrates the charge and discharge patterns of the HS system. It can be observed that hydrogen is primarily stored during low electricity price periods and discharged during peak price hours, aligning with the cost-minimization strategy. SOT is displayed in Fig. 3.21(b). The quantity of hydrogen in tank shows hydrogen reserves gradually increasing during the daytime and depleting as energy is discharged in the evening.

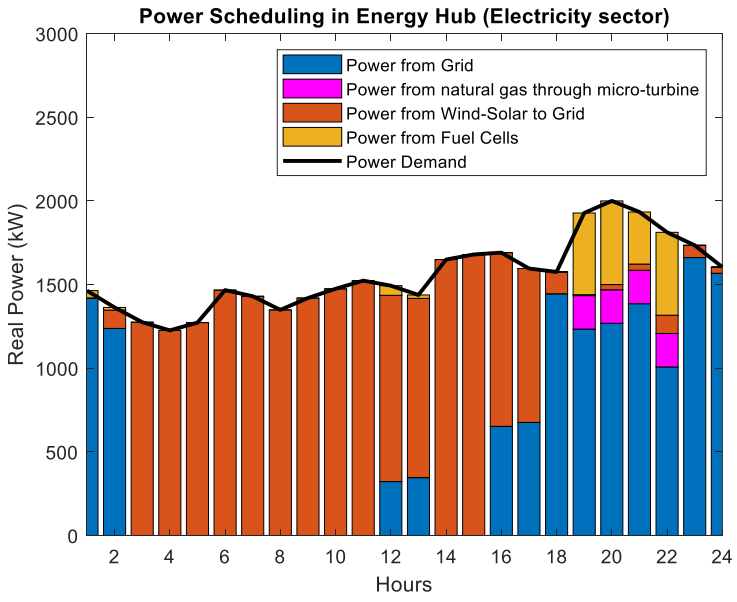

Figure 3.19 Power scheduling in EH under RTP scheme (electricity sector)

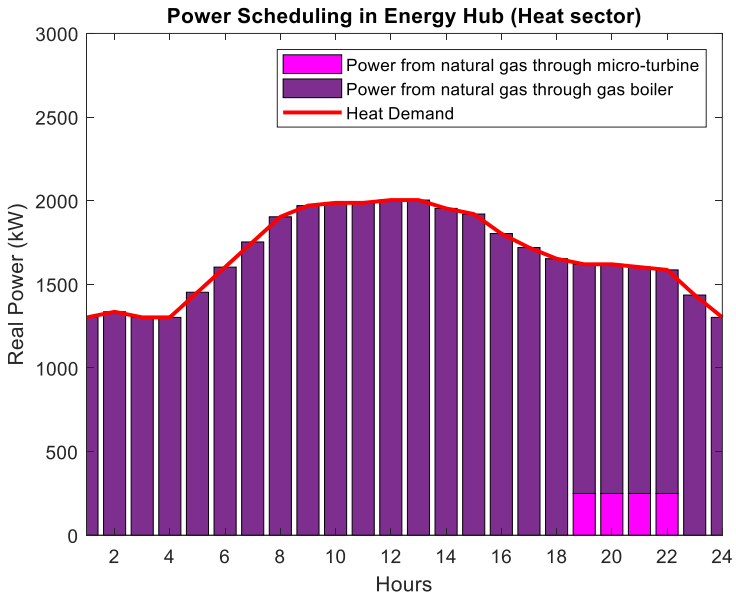

Figure 3.20 Power scheduling in EH under RTP scheme (heat sector)

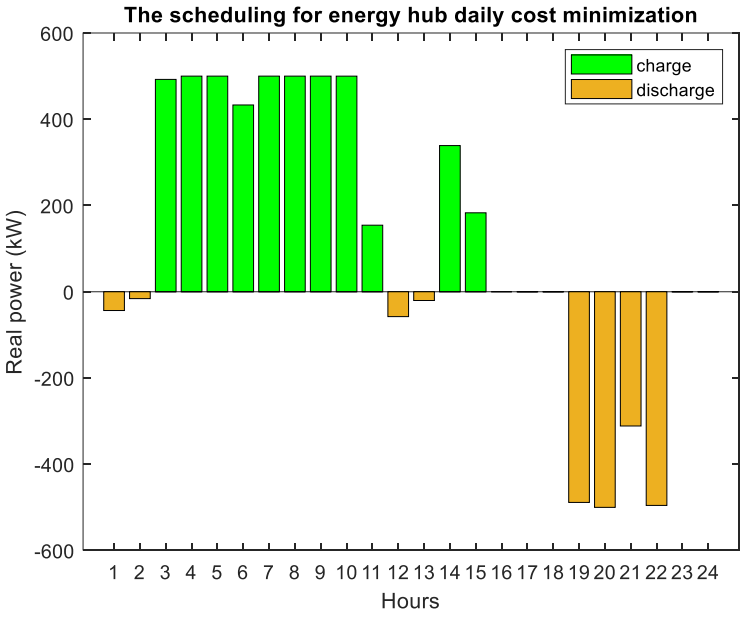

(a)

Figure 3.21 (a) HS scheduling for 24 hours and (b) State of the tank (%SOT) under RTP scheme

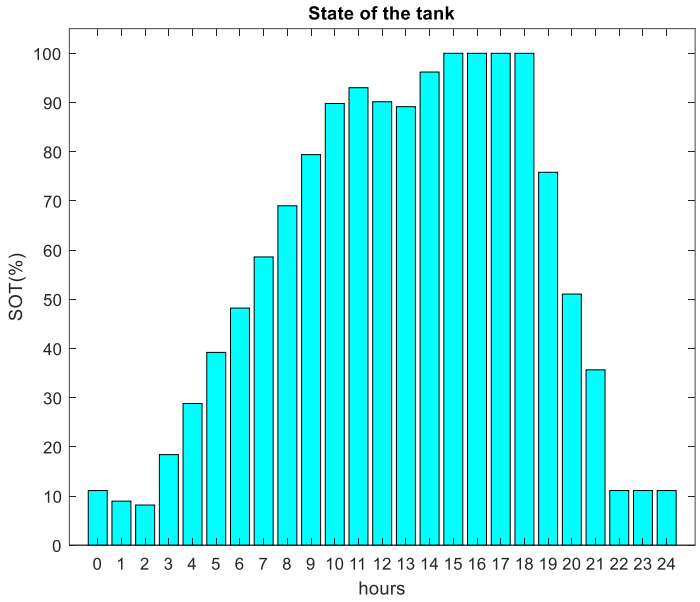

(b)

Figure 3.21 (a) HS scheduling for 24 hours and (b) State of the tank (%SOT) under RTP scheme (Continued)

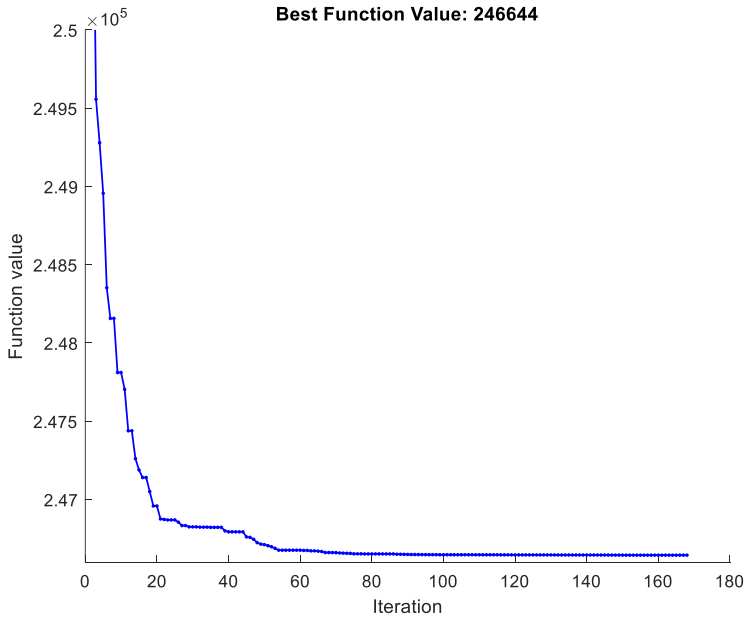

(a)

Figure 3.22 The PSO-LP (a) convergence plot and (b) fitness results with 30 iterations under RTP scheme

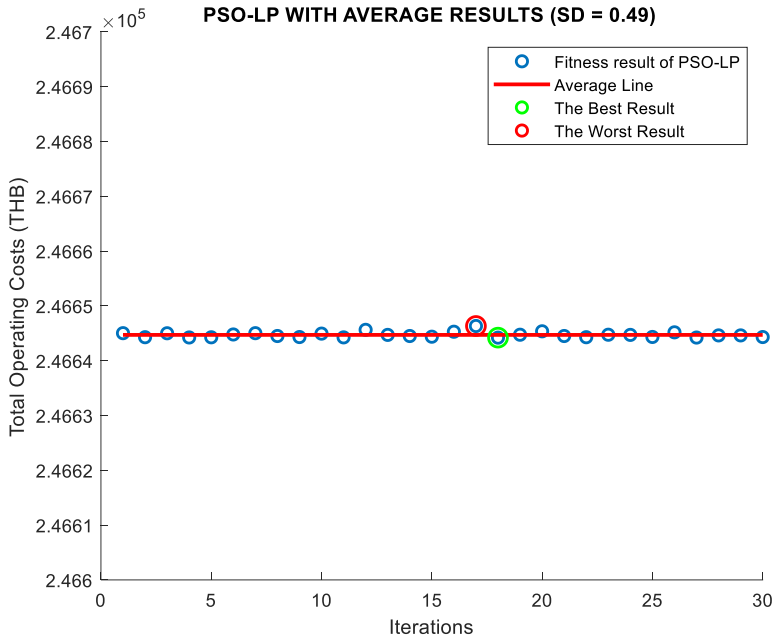

(b)

Figure 3.22 The PSO-LP (a) convergence plot and (b) fitness results with 30 iterations under RTP scheme (Continued)

Figure 3.22 (a) and (b) demonstrate the results from 30 trials of MES-WSPHS under RTP which show the best, worst, and average lines of solutions, indicate that the fitness results of PSO-LP are clustered, with the SD of 0.49. This study is reliable and has the potential to find optimal solutions more than TOU tariff.

3.4.4 The Comparison Between PSO and PSO-LP

This section illustrates a different solution between the PSO and PSO-LP technique under the TOC as an objective function and demonstrated in Case V. The aim is to highlight the performance of each approach that can minimize TOC effectively. To ensure a fair comparison between algorithms, the study established consistent parameters, as outlined in Table 3.5.

Table 3.5 The parameters of the PSO and PSO-LP settings

Variable	**Settings**
Swarm sizes	100
Iterations	500
Function Tolerance	$<10^{-6}$
w	[0.1,1.1]
c_1	1.49
c_2	1.49
$rand_1, rand_2$	[0,1]

Figure 3.23 presents a comparison between PSO and PSO-LP, illustrating that both algorithms demonstrate similar convergence behavior. However, the proposed PSO-LP terminates the optimization process at 285 iterations, due to the predefined convergence criteria based on the tolerance between the current particle swarm and the previous swarm, with a function tolerance of less than 10^{-6}. This enables PSO-LP to achieve a near-optimal global solution. In contrast, PSO requires 291 iterations to terminate, taking slightly longer and failing to reach a near-optimal solution. On the other hand, PSO-LP requires significant computational resources due to its two-step process: running PSO in the main loop and executing LP as a subroutine. This results in a longer runtime for PSO-LP compared to conventional PSO. Nevertheless, both algorithms are suitable for this problem, as the scheduling process must be completed within a day. The runtime details for this study are provided in Table 3.6.

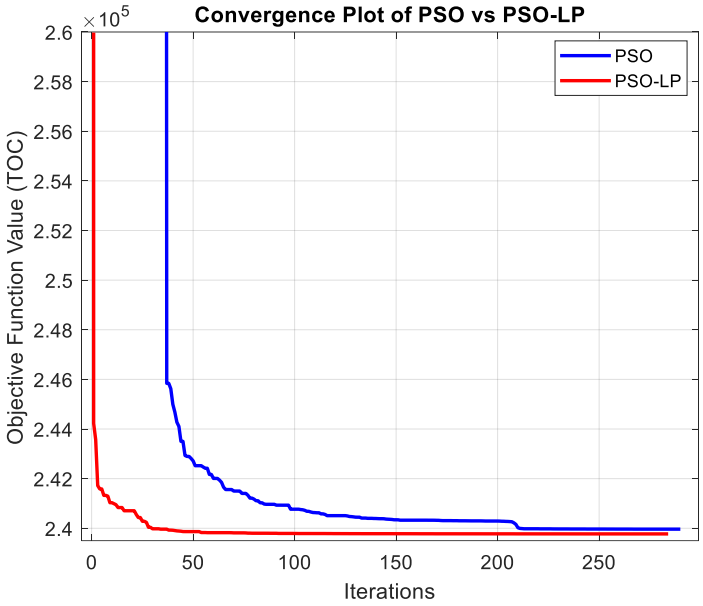

Figure 3.23 Convergence comparison between PSO and PSO-LP

Table 3.6 The runtime of the PSO and PSO-LP

Algorithm	PSO	PSO-LP
Runtime (s)	611	3,000

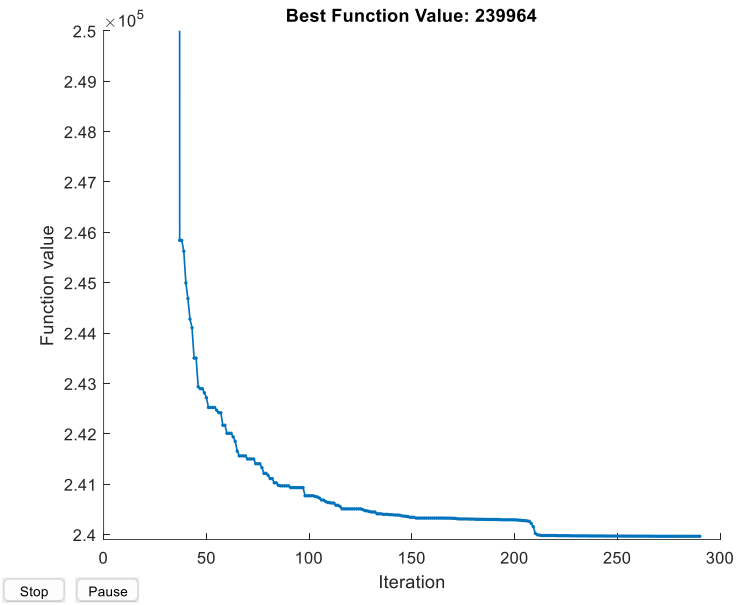

Figure 3.24 The PSO convergence plot

The PSO convergence plot in Fig. 3.24 indicates a final TOC value of 239,964 THB, whereas the PSO-LP convergence plot in Fig. 3.17 (c) shows a final TOC value of 239,772 THB. This comparison highlights that PSO-LP achieves a more optimal solution than the conventional PSO algorithm.

3.4.5 The Percentage of Multi-Energy Usage

This section presents the proportion of energy consumption from various sources within MES, which typically includes electricity from the grid, RE (wind and solar energy), and NG. Understanding the percentage contribution of each energy source offers valuable insights into the system's operational efficiency, sustainability, and its reliance on non-renewable energy sources. The results reflect that energy usage aligns with PDP2018, which emphasizes electricity and NG as the primary energy sources, while RE serves as an alternative to reduce carbon emissions. To further enhance the clarity of energy distribution, a pie chart is presented to visually illustrate the total energy consumption by source during the simulation, providing an intuitive understanding of each source's role within the system as shown in Fig. 3.25.

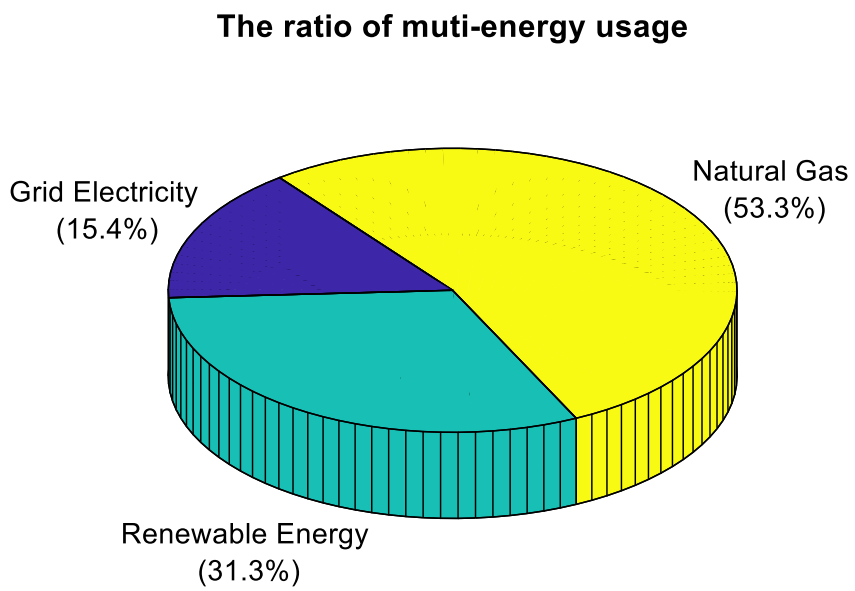

Figure 3.25 The energy consumption distribution among different sources for Case V

Based on the results, Case V is selected for this analysis as it demonstrates the most integrated operation among all the tested scenarios, showcasing the synergistic contribution of all available energy sources grid electricity, RE, NG, and hydrogen. The energy consumption ratio illustrates a diverse mix of sources, with a relatively modest contribution from RE. While fossil-based sources such as grid electricity and NG remain dominant, increasing the share of renewable energy is strongly recommended. A higher penetration of renewables can lead to significant long-term cost savings by reducing dependency on fuel-based sources, while simultaneously decreasing carbon dioxide emissions. Moreover, with effective energy scheduling and integration of storage systems like hydrogen, the variability of renewables can be managed efficiently. Therefore, future energy planning should prioritize renewable expansion to enhance sustainability, economic performance, and environmental benefits.

3.5 Chapter Summary

This chapter presented an optimized scheduling approach for OMES-WSPHS under a pricing mechanism aimed at minimizing the TOC. The study introduced a hybrid PSO-LP optimization method to enhance system efficiency by optimizing energy dispatch while considering TOU tariffs and RTP schemes. The simulation results demonstrated that integrating HS significantly enhances energy flexibility, particularly in balancing excess renewable including solar and wind power generation and peak demand periods. Comparing different operational scenarios, it is revealed that coordinated electricity and NG operations, along with HS, provide the lowest operating costs. Among the tested cases, Case V, which included both HS and coordinated energy dispatch, achieved the best determination of the objective function as TOC under the TOU scheme. When comparison between every case study, TOC decreased to a maximum of 4.58% compared to Case I (base case). Additionally, Under the RTP scheme, the coordination between energies is rescheduled to respond to dynamic

pricing scheme, leading to flexible operation with economic consideration. Moreover, the comparison between conventional PSO and the proposed PSO-LP method highlighted the advantages of incorporating linear programming in refining the optimization process. Although PSO-LP required higher computational resources, it converged to a more optimal solution with lower TOC compared to conventional PSO. Overall, the findings confirm that the proposed optimization framework effectively reduces operational costs while improving energy utilization and system flexibility.